



PCCP

Ionic transport in highly concentrated lithium bis(fluorosulfonyl)amide electrolytes with keto ester solvents: Structural implications for ion hopping conduction in liquid electrolytes

Journal:	<i>Physical Chemistry Chemical Physics</i>
Manuscript ID	CP-ART-01-2019-000425.R1
Article Type:	Paper
Date Submitted by the Author:	05-Feb-2019
Complete List of Authors:	Kondou, Shinji; Yokohama National University, Chemistry and Biotechnology Thomas, Morgan; Yokohama National University, MANDAI, Toshihiko; Iwate Daigaku, mandai@iwate-u.ac.jp Ueno, Kazuhide; Yokohama National University, Department of Chemistry and Biotechnology Dokko, Kaoru; Yokohama National University, Department of Chemistry and Biotechnology Watanabe, Masayoshi; Yokohama National University, Chemistry and Biotechnology

SCHOLARONE™
Manuscripts

Phys. Chem. Chem. Phys.

Ionic transport in highly concentrated lithium bis(fluorosulfonyl)amide electrolytes with keto ester solvents: Structural implications for ion hopping conduction in liquid electrolytes

Shinji Kondou,^a Morgan L. Thomas,^a Toshihiko Mandai,^b Kazuhide Ueno,^{*,a} Kaoru Dokko,^a and

Masayoshi Watanabe^a

^a Department of Chemistry and Biotechnology, Yokohama National University, 79-5 Tokiwadai, Hodogaya-ku, Yokohama 240-8501, Japan

^b Department of Chemistry and Biological Science Studies in Chemistry, Iwate University, Ueda 4-3-5, Morioka, 020-8551, Japan

CORRESPONDING AUTHOR FOOTNOTE: To whom correspondence should be addressed.
Telephone/Fax: +81-45-339-3951. E-mail: ueno-kazuhide-rc@ynu.ac.jp

Abstract

Recent studies have suggested that a Li ion hopping or ligand- or anion-exchange mechanism is largely involved in Li ion conduction of highly concentrated liquid electrolytes. To understand the determining factors for the Li ion hopping/exchange dominant conduction in such liquid systems, ionic diffusion behavior and Li ion coordination structures of concentrated liquid electrolytes composed of lithium bis(fluorosulfonyl)amide (Li[FSA]) and keto ester solvents with two carbonyl coordinating sites of increasing intramolecular distance (methyl pyruvate (MP), methyl acetoacetate (MA), and methyl levulinate (ML)) were studied. Diffusivity measurements of MP- and MA-based concentrated electrolytes showed faster Li ion diffusion than the solvent and FSA anion, demonstrating that Li ion diffusion was dominated by the Li ion hopping/exchange mechanism. A solvent-bridged, chain-like Li ion coordination structure as well as highly aggregated ion pairs (AGG) or ionic clusters e.g. $\text{Li}_x[\text{FSA}]_y^{(y-x)-}$ forming in the electrolytes were shown to contribute to Li ion hopping conduction. By contrast, ML, with greater intramolecular distance between the carbonyl moieties, is more prone to form a bidentate complex with a Li cation, which increased the contribution of the vehicle mechanism to Li ion diffusion even though similar AGG and ionic clusters were also observed. The clear correlation between the unusual Li ion diffusion and the solvent-bridged, chain-like structure provides an important insight into the design principles for fast Li ion conducting liquid electrolytes that would enable Li ion transport decoupled from viscosity-controlled mass transfer processes.

Introduction

Li ion conducting electrolytes are a key component of lithium rechargeable batteries. To accelerate widespread use of electric vehicles and other energy storage applications, there are intense research efforts on novel electrolyte materials with improved thermal and electrochemical stabilities and high ionic conductivity. Of particular importance are fast Li ion conducting materials for developing a high-power and fast-charging battery systems. In this context, superionic, inorganic solid-state electrolytes, wherein ion transport occurs solely by Li ion hopping conduction, have gained much interest since state-of-the-art solid-state electrolytes rival liquid electrolytes in conductivity ($10^{-3}\sim 10^{-2}$ S cm $^{-1}$) and possess single Li ion conduction behavior (i.e., Li transference number, $t_{\text{Li}} \sim 1$).^{1, 2} Indeed, a solid-state battery with sulfide-based superionic conductors demonstrated stable cycle performance and very fast charge-discharge operation, even within three minutes.³ However, constructing an effective electrolyte/electrode interface remains a critical challenge to the manufacture of large-scale solid-state cells for practical applications.

Highly concentrated liquid electrolytes have also drawn attention as prospective electrolyte materials for high-performance batteries.⁴ Near-saturation salt concentrations result in the scarcity of uncoordinated solvents in the electrolytes, improving the thermal and electrochemical stabilities.^{5, 6} Highly concentrated electrolytes also offer promise as electrolyte materials for high energy and power density cells: they enable higher rate charge-discharge performance of Li-ion batteries and more stable charge-discharge cycling of the metallic Li anode, compared with conventional organic liquid electrolytes.⁷⁻¹²

Although the basic assumptions underlying models of the ion transport processes in liquid

electrolyte rely predominantly on simple physical diffusion of ions according to the Stokes-Einstein relationship, recent molecular dynamics simulation studies predicted that Li ion hopping or exchange mechanisms through frequent exchange of solvent and anion with labile Li ion coordination can contribute to the ionic conduction of highly concentrated electrolytes.¹³⁻¹⁵ Despite low ionic conductivity and high viscosity, stable cycling of Li and Na ion batteries with high current density was reported for ionic liquid (IL)-based concentrated electrolytes. The improved rate capability was considered to be influenced by the increased mass transfer via ion hopping or exchange mechanisms through large ionic aggregates ($\text{Li}_m^+ \text{X}_n^-$) present in the IL-based concentrated electrolytes.¹⁶⁻¹⁸

In our previous work, diffusivity measurements by pulsed-field gradient (PFG-) NMR have shown that Li ions diffuse the fastest among the components (i.e. more rapidly than solvent molecules and anions) in sulfolane (SL)-based highly concentrated electrolytes.¹⁹ Here we note that another group also reported the fastest diffusion of Li ion in SL-based concentrated electrolytes.²⁰ This provides clear experimental evidence to suggest that Li ion hopping or exchange mechanisms make a significant contribution to Li ion diffusion. This unusual behavior was attributed to a unique Li ion coordination structure, where the two oxygen atoms of the SL SO_2 group coordinate to two different Li cations forming a SL-Li⁺-SL alternating chain structure. This finding motivated us to further elucidate the determining factors of the hopping/exchange-dominated Li ion conduction in liquid electrolytes.

Although the requisite molecular design and coordination structure were not understood in detail, we hypothesized that a solvent having multiple coordinating sites, with some degree of geometric/spatial-hindrance of multidentate coordination, forms a solvent-bridged, ionic network structure at high salt concentrations, and that can give rise to the hopping/exchange-dominated Li ion

conduction. In this study, keto ester compounds, methyl pyruvate (MP), methyl acetoacetate (MA), and methyl levulinate (ML), with zero, one or two methylene groups between the two carbonyl groups, respectively, were chosen as the solvents (**Figure 1**), and effects of solvent molecular structure on ionic diffusion was studied for highly concentrated electrolytes comprised of these solvents and lithium bis(fluorosulfonyl)amide (Li[FSA]). Li ion diffusion was found to be the fastest in shorter MP- and MA-based electrolytes, whereas the highest self-diffusion coefficient was observed for the anion in ML-based electrolytes. To unravel the origin of the different ionic diffusion behavior in the keto ester-based concentrated electrolytes, the coordination structure of the Li ions was studied with single crystal X-ray crystallography and Raman spectroscopy and correlations between the ionic diffusion behavior and the coordination structure were discussed.

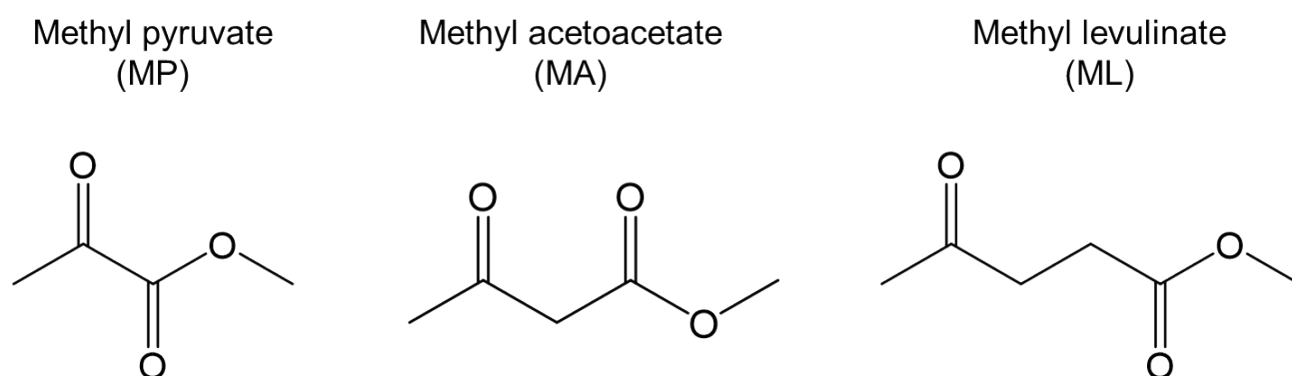


Figure 1. Chemical structure of keto ester solvents.

Experimental

Materials

Lithium bis(fluorosulfonyl)amide (Li[FSA]) was purchased from Kishida Chemical Co. (Japan) and used as received. Lithium bis(trifluoromethanesulfonyl)amide (Li[TFSA]) was kindly supplied by Solvay Japan. Methyl pyruvate (MP), methyl acetoacetate (MA), and methyl levulinate (ML) were purchased from Tokyo Chemical Industry Co. (Japan) and were dried over molecular sieves (3A) prior to use. The sample electrolytes were prepared by mixing Li[FSA] and the solvent at the appropriated ratio in an Ar-filled glove box (VAC, [H₂O] < 1 ppm, [O₂] < 1 ppm).

Measurement

The ionic conductivity (σ) of samples was determined by the complex impedance method using an impedance analyzer (VMP, Biologic) in the frequency range of 500 kHz-1 Hz with a sinusoidal alternating voltage amplitude of 10 mV root-mean-square (rms). A two platinized platinum electrodes cell (CG-511B, TOA Electronics) was utilized for the conductivity measurements, and the cell constant was determined using a 0.01 M KCl aqueous solution at 25 °C prior to the measurements. The density and viscosity were determined using a viscometer (SVM 3000, Anton Paar), and lithium salt concentration (c_{Li}) was determined from the density value at 30 °C and the molecular weight of the electrolytes.

The glass transition temperature (T_g) was determined using a differential scanning calorimeter (DSC7020, Hitachi High-Tech Science). The samples were hermetically sealed in aluminum pans. The samples were first heated to 60 °C, followed by cooling to -150 °C, and then reheated from -150 °C to 60 °C at a scan rate of 5 °C min⁻¹ under a nitrogen atmosphere.

PFG-NMR measurements were carried out to determine the self-diffusion coefficients of solvent (MP, MA, ML), Li⁺, and [FSA]⁻ using a bipolar pulse-pair longitudinal eddy current delay

(BPP-LED) pulse sequence with sinusoidal PFG.^{21, 22} A JEOL-ECX 400 NMR spectrometer with a 9.4 T narrow-bore superconducting magnet equipped with a pulsed-field gradient probe and current amplifier was used for the measurements: the solvents (¹H, 399.7 MHz), FSA anions (¹⁹F, 376.1 MHz), and lithium cations (⁷Li, 155.3 MHz). The sample was inserted into an NMR microtube (BMS-005J Shigemi) to a height of 3 mm to exclude convection, and the measurements were performed at 30 °C.

Raman spectra were measured using a Raman spectrometer with a 785 nm laser (NRS-4100, JACSO) and the instrument was calibrated using a polypropylene standard before the measurements. The spectroscopic resolution was 4.6 cm⁻¹. The samples were sealed in a capillary tube, and their temperature was controlled using a Peltier microscope stage (TS62, INSTEC) with a temperature controller (mk1000, INSTEC).

Density functional theory (DFT) and quantum calculations were performed using the Gaussian 09 program.²³ The geometries of complexes of Li ions and the keto ester solvents were optimized at the B3LYP/6-311+G* level, and vibrational analysis of the optimized structures was further performed at the same level.

Single crystal X-ray structure analysis was performed on a Rigaku XtaLAB PRO diffractometer using monochromatic Mo K α radiation ($\lambda = 0.71073$ Å). Single crystals were grown from the corresponding molten solvates in a cooling incubator (-10 °C). The single crystals were coated with vacuum grease to prevent contact with air, and mounted on a glass pin. The diffraction was measured at -50 °C using a steady flow of nitrogen gas stream. An empirical absorption correction was applied to the obtained data using spherical harmonics, implemented in the SCALES3 ABSPACK scaling

algorithm (CrysAlisPro 1.171.39.46e, Rigaku Oxford Diffraction, 2018). The crystallographic structure was solved by SHELXT 2018/2 and all non-hydrogen atoms were refined anisotropically by the full-matrix least-squares method (SHELXL 2018/3).²⁴ All the hydrogen atoms were placed in geometrically ideal positions and refined using the riding model.

Result and Discussion

Transport properties

Simple diketone-based solvents, such as diacetyl and acetyl acetone, were found to be relatively unstable for preparing the highly concentrated electrolytes of Li[FSA] in our preliminary tests. Therefore, chemically more stable keto esters were used as the solvents in this study. The keto ester-based highly concentrated electrolytes were prepared by mixing Li[FSA] and the solvents (MP, MA, or ML), and the prepared samples remained wholly liquid at room temperature, except for Li[FSA]:MP = 1:0.6. As with the reported concentrated electrolytes using FSA-based salts,²⁵⁻²⁸ the high Li salt solubility and the glass-forming properties may have their origin in the molecular flexibility of the FSA anions rendering its salts or complexes difficult to crystallize. **Table 1** summarizes the lithium salt concentrations (c_{Li}), viscosities (η), ionic conductivities (σ), self-diffusion coefficients of the components (D_{sol} , D_{Li} , and D_{FSA}), and glass transition temperatures (T_{g}) of the keto ester-based highly concentrated electrolytes (1:1 equimolar molar ratio of Li[FSA] and the solvent) at 30 °C. It is not surprising to note in **Table 1** that MP- and ML-based electrolytes are relatively viscous liquids with η exceeding 1000 mPa s at 30 °C, leading to the relatively low σ of 10^{-4} S cm⁻¹. The MA-based electrolyte showed a one-order of magnitude lower η , and higher σ and diffusion constants even

with its intermediate c_{Li} and T_{g} . The reason for the exceptionally low viscosity is not clear at present.

More interestingly, either D_{Li} or D_{FSA} is the highest among the diffusion constants measured for all the components, suggesting that the ionic species (namely, Li^+ or $[\text{FSA}]^-$) can diffuse faster than the solvent. Li^+ ions are the most mobile in the MP- and MA-based electrolytes whereas FSA anions diffuse the fastest in the ML-based electrolyte. These observations are contrary to the situation in conventional electrolyte solutions. In typical organic liquid electrolytes with 1 mol dm^{-3} of Li salt, the self-diffusion coefficients follow the order: $\text{Li}^+ < \text{anion} < \text{solvents}$.^{29, 30} Despite the smallest size of isolated Li ions, D_{Li} is smaller than D_{sol} as a consequence of the larger hydrodynamic radius of the ‘solvated’ Li ions, in reference to the Stokes-Einstein relationship.

In our previous work, it was found that the same holds true for highly concentrated, molten complex electrolytes of lithium bis(trifluoromethanesulfonyl)amide ($\text{Li}[\text{TFSA}] > 3 \text{ mol dm}^{-3}$) in tetrahydrofuran (THF), 1,2-dimethoxyethane (DME), and dimethyl sulfoxide (DMSO) where the solvent molecules diffuse faster than the ions.^{31, 32} Moreover, a higher diffusion coefficient of water than the component ions of the Li salt, and physical diffusion of hydrated Li ions were also reported for molten salt hydrate electrolytes, determined by diffusivity measurements combined with molecular dynamic simulations.³³ It should be noted that specific cases have been observed for other molten complexes of $\text{Li}[\text{TFSA}]$ and multidentate oligoether solvents such as triglyme (G3) and tetraglyme (G4). In the equimolar complexes of $\text{Li}[\text{TFSA}]$ and G3 or G4 (so-called solvate ionic liquids), D_{Li} is found to be identical to D_{sol} , indicating that long-lived Li complex ions are formed due to strongly chelating properties of G3 and G4.³² Nevertheless, in the glyme-Li salt solvate ionic liquids, the Li ion transport can generally be interpreted as being via the physical diffusion mechanism that premises the

translational motion of the solvated ions in a similar manner as for ionic liquids³⁴ as well as dilute electrolyte solutions.²⁹ In contrast to these examples, the diffusion behavior observed for the highly concentrated Li[FSA]/keto ester systems is more akin to our recently published observations for SL-based concentrated electrolytes.¹⁹

Table 1. Lithium salt concentrations (c_{Li}), viscosity (η), ionic conductivity (σ), self-diffusion coefficient of the components (D_{sol} , D_{Li} , and D_{FSA}), and glass transition temperature (T_{g}) of Li[FSA]:MP=1:1, Li[FSA]:MA=1:1, and Li[FSA]:ML=1:1 at 30 °C.

Molar ratio	c_{Li}	η	σ	D_{sol}	D_{Li}	D_{FSA}	T_{g}
1:1	mol dm ⁻³	mPa s	mS cm ⁻¹	$\times 10^{-7}$ cm ² s ⁻¹	$\times 10^{-7}$ cm ² s ⁻¹	$\times 10^{-7}$ cm ² s ⁻¹	°C
Li[FSA]:MP	5.58	1220	0.43	0.20	0.21	0.16	-43.7
Li[FSA]:MA	5.08	270	1.51	0.61	0.70	0.60	-53.3
Li[FSA]:ML	4.69	1030	0.37	0.13	0.15	0.18	-62.9

Figure 2 shows the diffusivity ratios of $D_{\text{sol}}/D_{\text{Li}}$ and $D_{\text{FSA}}/D_{\text{Li}}$ in the concentrated electrolytes with various [solvent]/[Li] ratios. As shown in **Figure 2a**, $D_{\text{sol}}/D_{\text{Li}}$ of all the samples was less than unity in the range of [solvent]/[Li] ratios studied. The lower $D_{\text{sol}}/D_{\text{Li}}$ at lower [solvent]/[Li] ratio indicates that the mobility of Li ions became even greater than that of the solvent molecules. Obviously, the keto ester-based concentrated electrolytes can be considered as exceptional with regard to ionic transport behavior when compared with typical liquid electrolytes. The lower $D_{\text{sol}}/D_{\text{Li}}$ for the ML-based electrolytes is probably attributable to the larger size of the ML molecules. In **Figure 2b**, $D_{\text{FSA}}/D_{\text{Li}}$

was also less than unity for MP- and MA-based electrolytes and decreased with decreasing [solvent]/[Li] ratio. The fastest Li ion transport in these electrolytes cannot be explained by the simple physical diffusion of Li ions because Li ion is unlikely to exist in ‘naked’ (unsolvated) form but should be stabilized by coordination by the donor sites of the solvents and counter anions. For ML-based electrolytes, $D_{\text{FSA}}/D_{\text{Li}}$ was greater than unity and the value approached unity at [solvent]/[Li] = 0.6, confirming that FSA anions are the fastest diffusive component in the electrolytes. The Li transference number (t_{Li}) estimated by the self-diffusion coefficient of the ions, $t_{\text{Li}} = D_{\text{Li}}/(D_{\text{Li}} + D_{\text{FSA}})$, marked a high value ranging from 0.54 to 0.60 for MP- and MA-based electrolytes, while t_{Li} was found to be lower than 0.5 for the ML-based electrolytes (See Electronic Supplementary Information ESI, **Figure S1**).

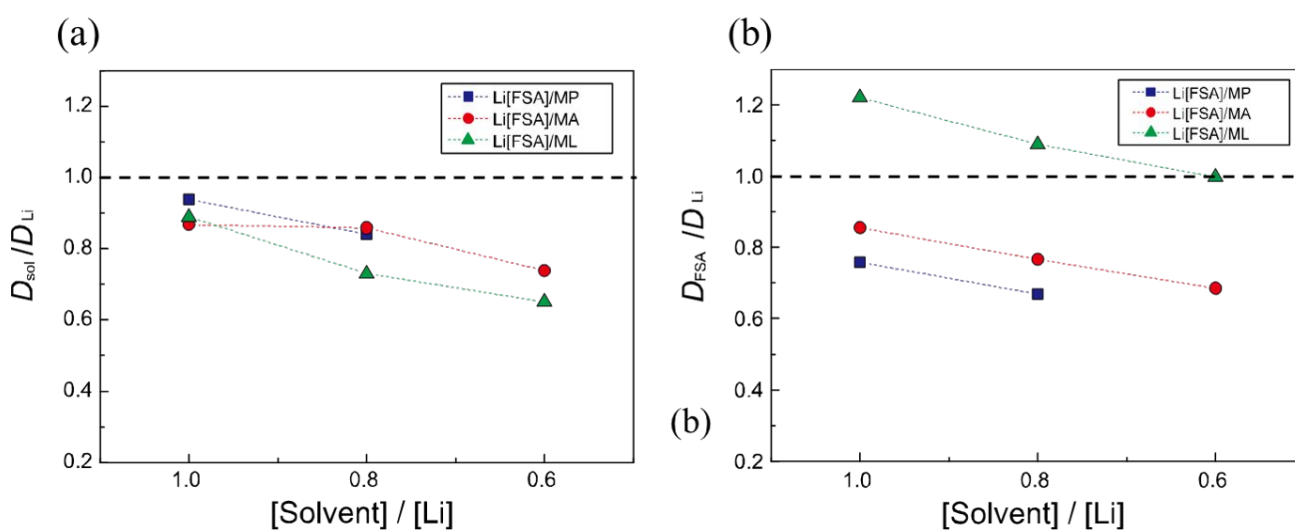


Figure 2. Diffusivity ratios of (a) $D_{\text{sol}}/D_{\text{Li}}$ and (b) $D_{\text{FSA}}/D_{\text{Li}}$ in the keto ester-based concentrated electrolytes of Li[FSA] at 30 °C.

The anomalous ionic diffusion behavior in the keto ester-based electrolytes may be attributed to transport mechanisms other than simple physical diffusion. In proton-conducting electrolytes, there is another mechanism proposed for proton transport in addition to the physical transport of hydronium

ions (known as the vehicle mechanism): the proton-hopping Grotthuss or structural diffusion mechanism, which relies on proton exchange reactions from one site to another through the hydrogen bond network in aqueous electrolytes.³⁵ Experimental evidence for ionic diffusion occurring faster than that of the solvents suggests that the ionic transport in keto ester-based electrolytes involves a Li ion hopping/exchange mechanism. Moreover, as shown in **Figure 2b**, there is an intriguing difference in the ionic transport behavior between MP- and MA-based electrolytes and ML-based electrolytes despite their structural analogy. The more-pronounced diffusion of Li ions for the former may result from predominant Li ion hopping or exchange between coordinating sites, which is akin to that which was observed for SL-based concentrated electrolytes.¹⁹ On the contrary, more frequent anion exchange reactions can be responsible for the fastest diffusion of FSA anions in the latter. We note here that similar diffusion behavior of FSA anions was also observed in highly concentrated electrolytes comprised of Li[FSA] in G3 or G4 when the Li[FSA] was in stoichiometric excess.²⁸ It can be conceived that these unusual ionic transport behaviors may correlate with a unique coordination structure in these dense electrolytes since an extended network structure plays an essential role in the proton-hopping Grotthuss-type mechanism.³⁵ Therefore, we subsequently studied how the subtle change in the molecular structure of the keto ester solvents affects the Li ion coordination, towards clarifying the origin of the observed difference in ionic transport behavior between MP- or MA-based electrolytes and ML-based electrolytes.

Coordination Structure

The Li ion coordination structures in the keto ester-based electrolytes were investigated with single

X-ray crystallography and Raman spectroscopy with the aid of DFT calculations. For MP-based electrolytes, a single crystalline sample could be obtained at $[MP]/[Li] = 0.5$ in which the Li salt concentration is slightly higher than the studied liquid electrolytes, and its crystal structure is shown in **Figure 3** and **Figure S2**. The Li ions are coordinated by a total of four or five oxygen atoms contributed from both MP and the FSA anions. MP molecules adopt a *s-cis* conformation, and the ketone carbonyl oxygen and the ester carbonyl oxygen atoms bind to different Li ions with a Li-O distance of ~ 1.95 Å. The ketone carbonyl oxygen also interacts with the Li ion that is coordinated by the ester carbonyl oxygen of the same MP molecules (i.e. as a bidentate ligand), but the Li-O distance is rather long (~ 2.53 Å). FSA anions adopt a C_1 (*cisoid*) conformation³⁶ and are coordinated to three different Li ions using three of the four oxygen atoms of the two sulfonyl groups, forming polymeric chains, $Li^+ \cdots FSA \cdots Li^+ \cdots FSA \cdots$. Furthermore, MP molecules and FSA anions form a joint polymeric cluster with the Li ion linkages, i.e. $\cdots MP \cdots Li^+ \cdots FSA \cdots Li^+ \cdots MP \cdots$.

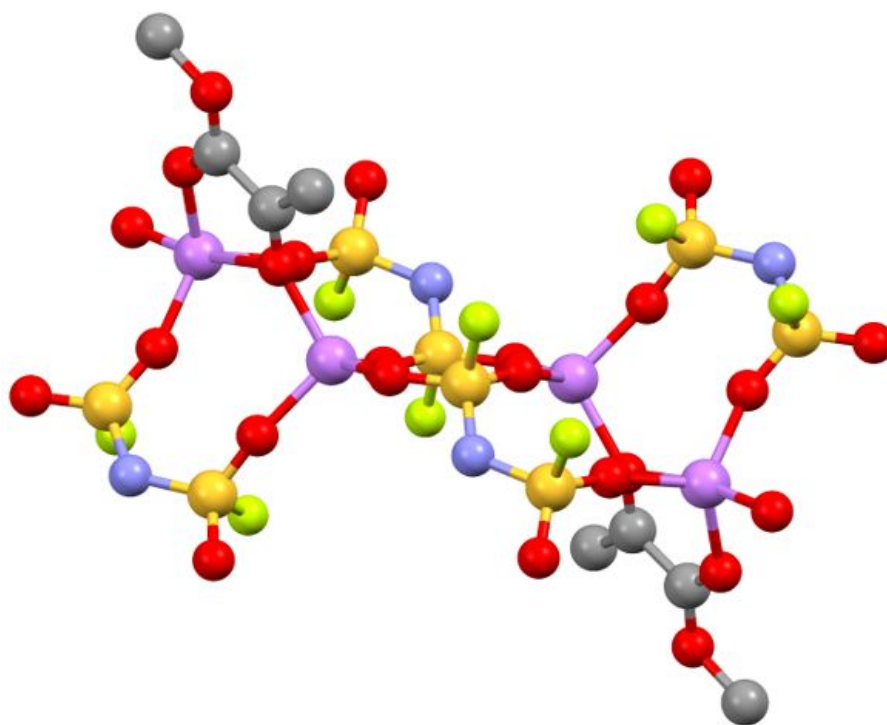


Figure 3. Ball and stick models for single crystal of MP-Li[FSA] solvate at $[MP]/[Li] = 0.5$. Hydrogen atoms are omitted for clarity. Purple, Li; red, O; gray, C; yellow, S; light green, F; light blue, N. The

crystallographic information file (cif) was deposited in the Cambridge Structure Database as CCDC 1886677.

Figure 4a shows Raman spectra in the region of 780-900 cm^{-1} for MP-based liquid electrolytes and solid complexes with Li[FSA]. The peak in the range of 810-880 cm^{-1} can be assigned to the mixed modes of C-C stretching, CH_3 rocking and C-O stretching vibrations of the methyl ester group,³⁷ and were found to be sensitive to Li salt concentration in our preliminary Raman experiments. By contrast, it was difficult to analyze the C=O stretching bands of ketone and ester groups (around 1700 cm^{-1}) on account of their complicated change and band overlap upon addition of Li salt (**Figure S3**). The crystalline solid of $[\text{MP}]/[\text{Li}] = 0.5$ exhibits a peak at 846 cm^{-1} , corresponding to the *s-cis* MP complex coordinated with two Li ions as found in the single crystal structure. This band was well reproduced by the vibrational analysis of the Li^+ -MP (2:1) complex extracted from the crystalline structure (**Figure 4b**). Another peak at 868 cm^{-1} was attributed to the additional presence of solid Li[FSA] in the crystalline sample used for collecting experimental Raman spectra (**Figure S4**). The MP-based electrolytes formed another solid solvate at $[\text{MP}]/[\text{Li}] = 2$, although we could not obtain a reliable crystallographic model with acceptable *R*-factor. However, the roughly refined model implies that two MP molecules coordinate in a co-planar bidentate manner with one Li ion, and the Li ion is further coordinated by an oxygen atom of the FSA anions from the top and bottom sides of the $[\text{Li}(\text{MP})_2]$ plane in the crystalline solvate (**Figure S5**). The $[\text{Li}(\text{MP})_2]$ coordination shows a relatively sharp Raman peak (**Figure 4a**) at 837 cm^{-1} with a small peak around 800 cm^{-1} , likely due to the two bidentate MP molecules in the form of the co-planar coordination as suggested by the corresponding theoretical bands at 833 and 807 cm^{-1} (**Figure 4c**). The asymmetric peak around 840 cm^{-1} for the

liquid electrolyte of $[\text{MP}]/[\text{Li}] = 1$ can be interpreted as resulting from the sum of the two aforementioned peaks (bridging MP at 846 cm^{-1} and bidentate MP at 837 cm^{-1}) found in the two solid solvates. A similar asymmetric peak was also observed for the molten (supercooled) state at $[\text{MP}]/[\text{Li}] = 0.5$ with a larger apparent contribution from the peak corresponding to the bridging MP (at 846 cm^{-1}). Therefore, MP-bridged ionic aggregates and the $[\text{Li}(\text{MP})_2]$ -like coordination are likely to coexist in the MP-based liquid electrolytes in the range of $[\text{MP}]/[\text{Li}] = 0.6$ to 1.

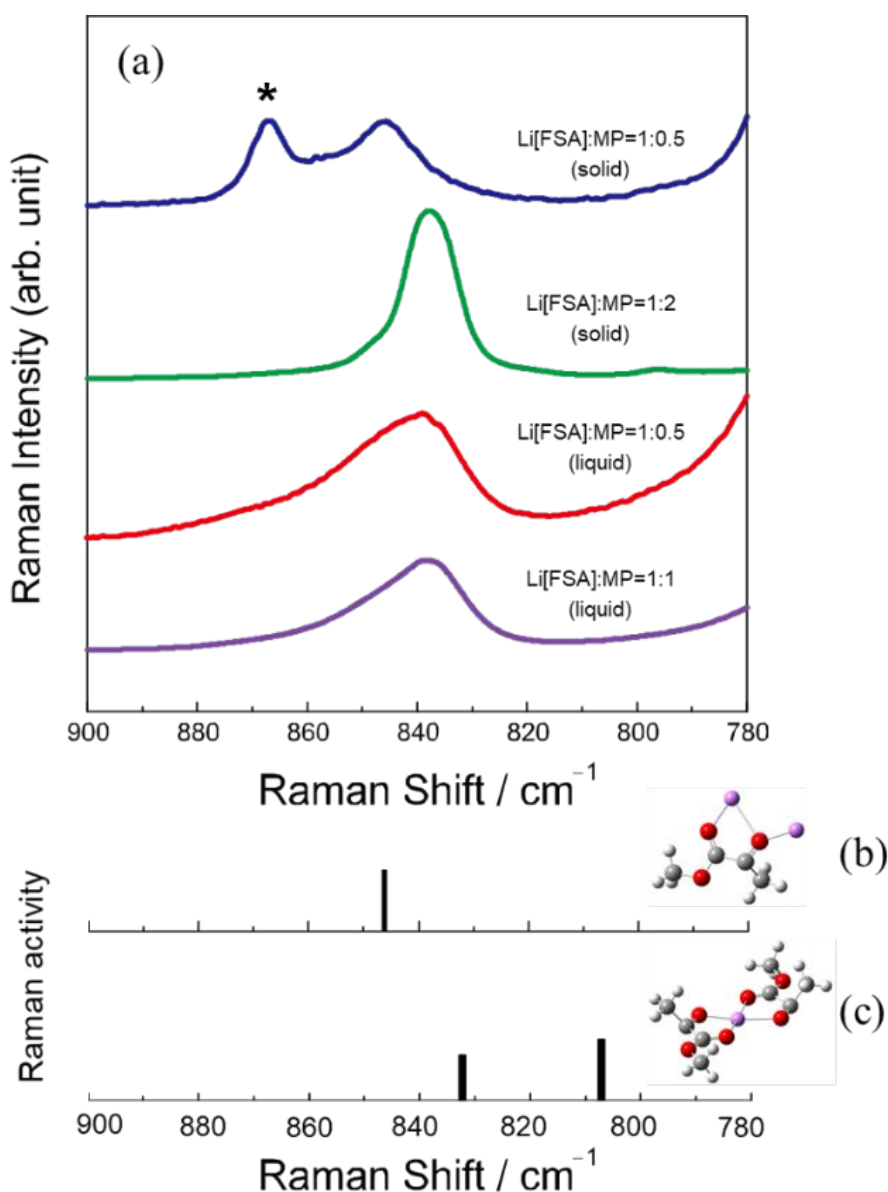


Figure 4. (a) Raman spectra of MP-based liquid electrolytes ($[\text{MP}]/[\text{Li}] = 1$) and solid or supercooled complexes ($[\text{MP}]/[\text{Li}] = 0.5, 1$ and 2) with Li[FSA], and theoretical Raman bands of (b) Li^+ -MP (2:1) complex extracted from the crystalline structure of the complex at $[\text{MP}]/[\text{Li}] = 0.5$ and (c) Li^+ -MP

(1:2) complex from the roughly refined crystal structure at $[\text{MP}]/[\text{Li}] = 2$, in the range of $780\text{--}900\text{ cm}^{-1}$ corresponding to the mixed modes of C-C stretching, CH_3 rocking and C-O stretching vibrations of the methyl ester group of MP. The peak (*) at 868 cm^{-1} is due to the Li[FSA] (solid) contained in the measured sample (see Figure S4 in ESI).

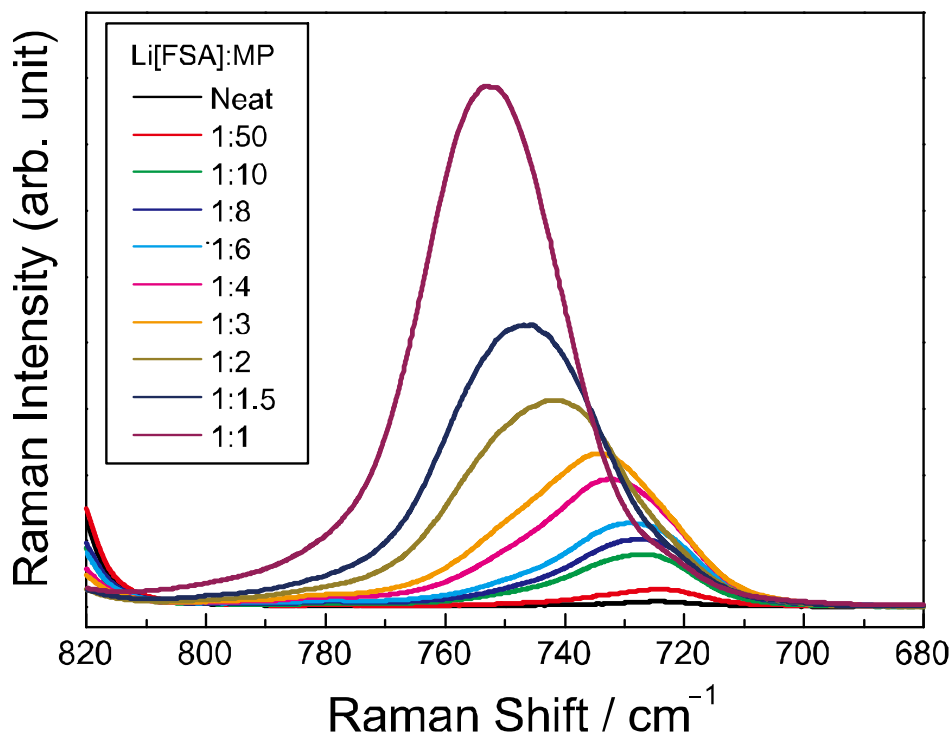


Figure 5. Raman spectra of MP-based liquid electrolytes at various Li[FSA]:MP ratios in the range of $680\text{--}820\text{ cm}^{-1}$ for the symmetric stretching vibration of the S-N-S skeleton of FSA anions.

The Raman bands in the range of $720\text{--}760\text{ cm}^{-1}$ correspond to the symmetric stretching vibration of the S-N-S skeleton of FSA anions and have been well studied for Li[FSA]-based electrolytes in organic solvents^{26,28} and ionic liquids.^{36,38} As seen in **Figure 5**, the peak continuously shifts from 720 cm^{-1} to 755 cm^{-1} with increasing Li salt concentration (i.e., decreasing $[\text{MP}]/[\text{Li}]$) in the MP-based liquid electrolytes. A systematic Raman study of AN/Li[FSA] systems has shown possible assignments of different ionic association states of FSA: $720\text{ to }726\text{ cm}^{-1}$ for uncoordinated anions, 735 cm^{-1} for contact ion pairs (CIP), and 741 cm^{-1} to 752 cm^{-1} for highly aggregated ion pairs (AGG).²⁶ A similar large Raman shift was also reported for *N*-propyl-*N*-methylpyrrolidinium bis(fluorosulfonyl)amide ($[\text{C}_3\text{mpyr}][\text{FSA}]$), mixed with Li[FSA]³⁸ and glyme/Li[FSA] systems.²⁸ In

these works, the broad Raman peak around 750 cm^{-1} in the high Li concentration regime was attributed to higher levels of ionic aggregates. Likewise, we can expect that AGG or multiple ionic clusters such as $\text{Li}_x[\text{FSA}]_y^{(y-x)-}$ were present in MP-based concentrated electrolytes at $[\text{MP}]/[\text{Li}]$ less than 1. As shown in **Figure S6**, Raman spectra of the MA-based and ML-based electrolytes also showed a similar peak shift from 720 cm^{-1} to 755 cm^{-1} with increasing Li salt concentration, and a broad Raman peak around 750 cm^{-1} at high Li concentration regime. Therefore, we assume that AGG or ionic clusters are formed in the keto ester-based highly concentrated electrolytes in the studied range of Li salt concentrations.

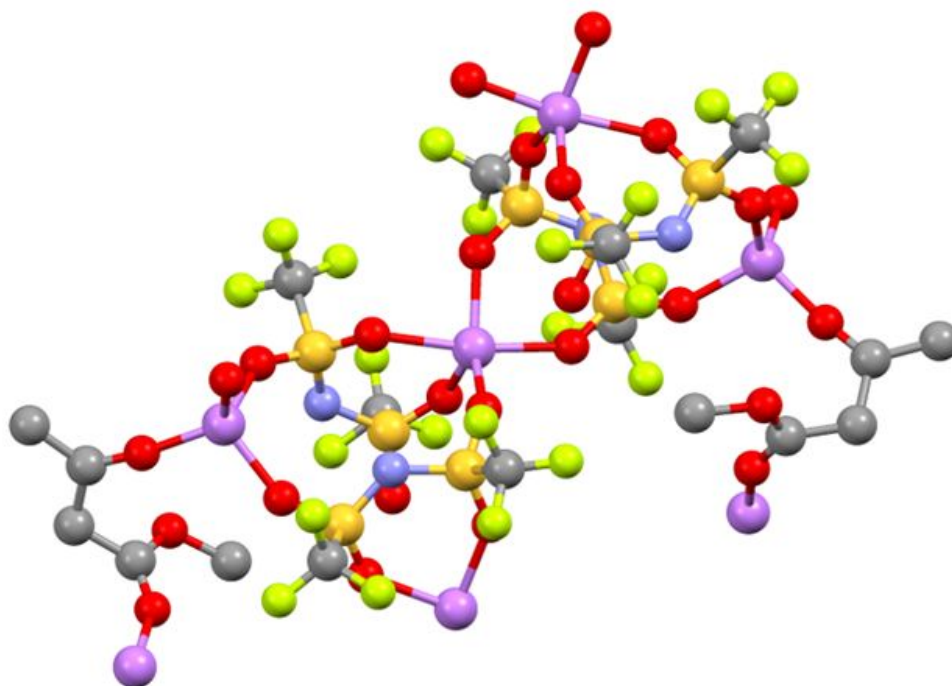


Figure 6. Ball and stick models for single crystal of MA-Li[TFSA] solvate at $[\text{MA}]/[\text{Li}] = 0.5$. Hydrogen atoms are omitted for clarity. Purple, Li; red, O; gray, C; yellow, S; light green, F; light blue, N. The crystallographic information file (cif) was deposited in the Cambridge Structure Database as CCDC 1892798.

For MA-based electrolytes, Raman spectra in the region of $1600\text{--}1800\text{ cm}^{-1}$ (for C=O stretching) suggested the presence of the enol form in addition to keto form due to keto-enol tautomerism in neat

MA solvent (**Figure S7**).³⁹ However, the peak at 1627 cm^{-1} corresponding to the enol form declined with addition of Li[FSA], and completely vanished at $[\text{MA}]/[\text{Li}]$ lower than 2, indicating that MA molecules exist entirely as the keto form in MA-based concentrated electrolytes, consistent with another study indicating the decreasing enol content of a β -keto ester with increasing alkali metal salt concentration.⁴⁰ Unfortunately, we could not obtain any crystalline solids adequate for X-ray crystallography over the range of $[\text{MA}]/[\text{Li}]$ studied. Instead, replacement of FSA anions by an analog, TFSA, allowed the MA-based electrolytes to form a fine crystal in the concentration region of our interest. **Figure 6 and S8** show the single crystal structure of the crystalline solvate at $[\text{MA}]/[\text{Li}] = 0.5$ for the MA-Li[TFSA] system. Similar to the MP-Li[FSA] solvate at $[\text{MP}]/[\text{Li}] = 0.5$, the ketone carbonyl oxygen and the ester carbonyl oxygen atoms of MA coordinate to different neighboring Li ions with Li-O distances of $1.86\text{--}1.91\text{ \AA}$. Again, MA molecules served as a linker to form a solvent-shared, extended ionic network $\cdots\text{MA}\cdots\text{Li}^+\cdots\text{TFSA}\cdots\text{Li}^+\cdots\text{MA}\cdots$ in the crystal at $[\text{MA}]/[\text{Li}] = 0.5$. TFSA anions in C_1 (cisoid) conformation coordinate to three Li ions. However, in contrast to the crystal structure of $[\text{MP}]/[\text{Li}] = 0.5$ (**Figure 3**), Li ions coordinated only by TFSA anions are also present, in addition to Li ions coordinated by both MA and TFSA. Furthermore, we found another crystal structure in the same sample at $[\text{MA}]/[\text{Li}] = 0.5$ (**Figure S9**) in which MA molecules have a little different conformation from that shown in **Figure 6**, but form a similar solvent-shared Li ion coordination structure. These polymorphs of the crystalline solvate at $[\text{MA}]/[\text{Li}] = 0.5$ were considered for the following discussion on Raman spectra.

In **Figure 7a**, Raman spectra in the region of $770\text{--}890\text{ cm}^{-1}$ for MA-based liquid electrolytes of Li[FSA] ($[\text{MA}]/[\text{Li}] = 1$) were compared with those for the crystalline and molten complexes with

Li[TFSA] ($[MA]/[Li] = 0.5$). The peak in the region of $810\text{-}890\text{ cm}^{-1}$ involves the mixed modes of C-C stretching, CH_3 rocking and C-O stretching vibrations of MA molecules,³⁹ and is sensitive to the conformational changes in the MA molecule upon Li coordination. **Figure 7b, c, d, and e** also show the theoretical Raman bands corresponding to possible Li ion coordination structures in MA-based electrolytes. The Raman band at 806 cm^{-1} is derived from TFSA anions for the crystalline and molten complexes with Li[TFSA]. The experimental Raman bands of the crystalline complex of $[MA]/[Li] = 0.5$ agree well with theoretical Raman bands of the $\text{Li}^+\text{-MA}$ (2:1) complex extracted from the crystalline structures at 802 and 813 cm^{-1} in **Figure 7b**, and 814 and 875 cm^{-1} in **Figure 7c**. The theoretical Raman band at 813 (**Figure 7b**) and 814 cm^{-1} (**Figure 7c**) shift to 830 cm^{-1} for the optimized $\text{Li}^+\text{-MA}$ (2:1) complex with the bridging structure (**Figure 7d**) and to 846 and 852 cm^{-1} for the optimized $\text{Li}^+\text{-MA}$ (1:1) complex with the bidentate structure (**Figure 7e**). The Raman spectrum of the MA-based liquid electrolyte of Li[FSA] ($[MA]/[Li] = 1$) was somewhat broader, probably due to the presence of different conformations of MA molecules in the liquid state. The broad peaks around 816 and 848 cm^{-1} indicate that the MA molecules adopt a variety of conformations including both bridging and bidentate structures. As a result, in the MA-based concentrated liquid electrolytes, it is suggested that both MA-bridged and FSA-bridged ionic aggregates would be present in addition to other Li-MA complexes with the bidentate form of MA.

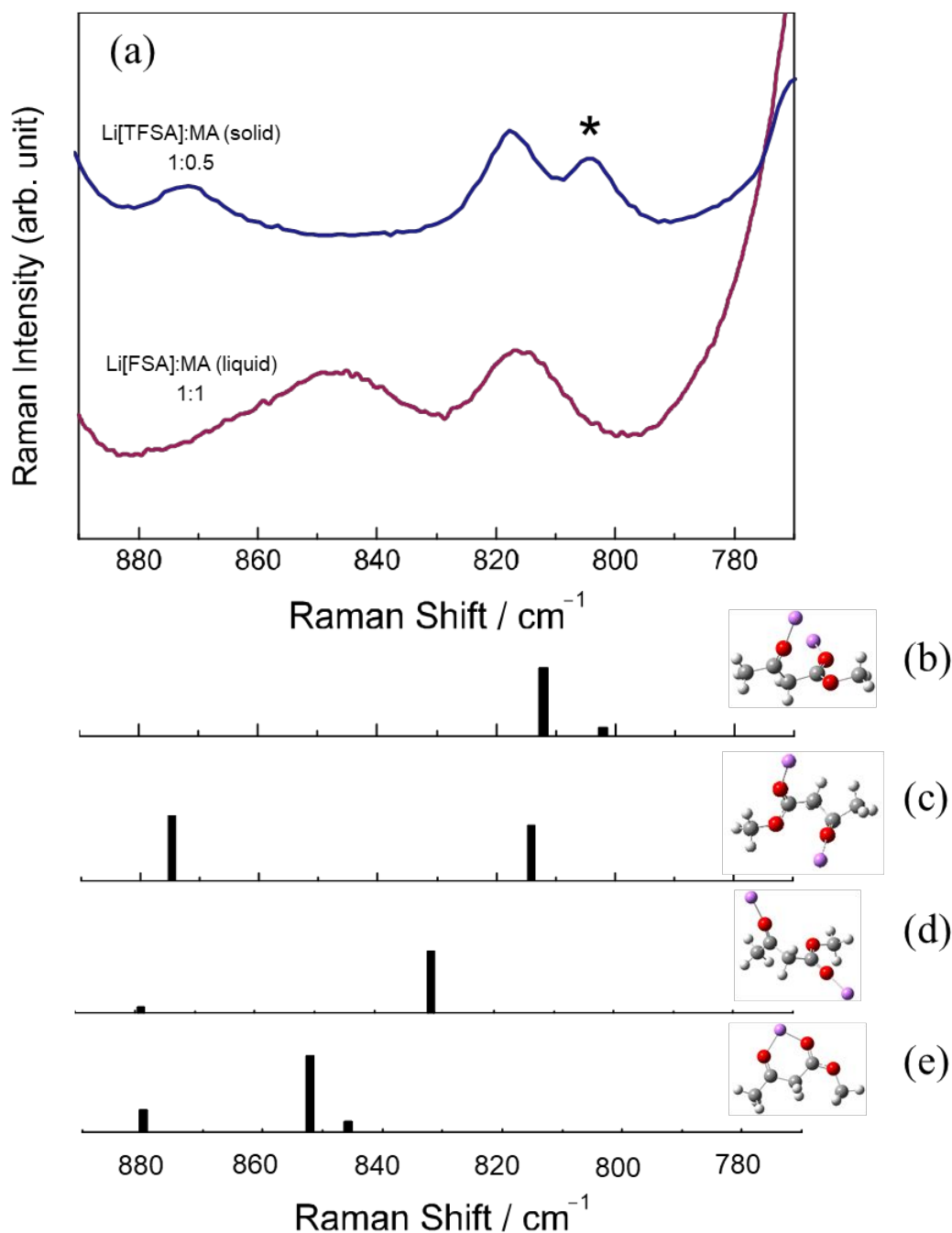


Figure 7. (a) Raman spectra of MA-based liquid electrolyte ($[MA]/[Li] = 1$) with Li[FSA] and solid complex ($[MA]/[Li] = 0.5$) with Li[TFSA], and theoretical Raman bands and corresponding structures of Li⁺-MA (2:1) complex extracted from the crystal structure (b) Figure 6 and (c) Figure S9. (d) optimized Li⁺-MA (2:1) bridging complex and (e) optimized Li⁺-MP (1:1) bidentate complex, in the range of 770-890 cm⁻¹ corresponding to the mixed modes of C-C stretching, CH₃ rocking and C-O stretching vibrations of MA. The peak (*) at 806 cm⁻¹ is derived from TFSA anions.

For ML-based concentrated systems, we could not obtain a high-quality crystal adequate for single X-ray crystallography with either Li[FSA] or Li[TFSA]. **Figure 8a** shows the concentration dependent Raman spectra in the range of 860-940 cm⁻¹. A characteristic peak corresponding to neat ML at 896 cm⁻¹, resulting from the mixed modes of C-C stretching, CH₃ rocking and C-O stretching vibrations,

was well reproduced by the DFT calculation (**Figure 8b**). With increasing salt concentration, the intensity of the peak at 897 cm^{-1} for neat ML decreased, but two peaks emerged at 870 and 910 cm^{-1} and their intensity increased. As seen in **Figure 8c**, these peaks at 870 and 910 cm^{-1} correspond to the bidentate form of the Li^+ -ML (1:1) complex. The DFT calculation predicted that the bridged Li^+ -ML (2:1) complex shows a Raman band at 896 cm^{-1} (**Figure 8d**), which is close to that of neat ML. In the experimental Raman spectrum for the ML-based concentrated electrolyte (1:1), the intensity around $890\text{-}900\text{ cm}^{-1}$ was very low, implying that both non-coordinating and bridging ML may be unlikely to exist or their fraction is very small: most of the ML molecules would adopt the bidentate form in ML-based concentrated electrolytes. It is likely that ML, with a greater intramolecular distance between the carboxyl groups, prefers conformationally to adopt a bidentate structure for coordinating to Li ions. A similar scenario can be derived from the Raman spectra in the range of $700\text{-}810\text{ cm}^{-1}$ (**Figure S10**). The Raman band at 767 cm^{-1} for neat ML decreases, and the band at 779 cm^{-1} for the bidentate ML was intensified with salt concentration. Again, Raman bands in this frequency region suggest that the non-coordinating (767 cm^{-1}) and bridging (765 cm^{-1}) species constitute only small fractions, and therefore the majority of ML may be present in the form of bidentate complexes. As suggested by the Raman band shift for FSA anions (**Figure S6**), Li ions and FSA anions formed AGG or ionic clusters in the ML-based concentrated electrolytes.

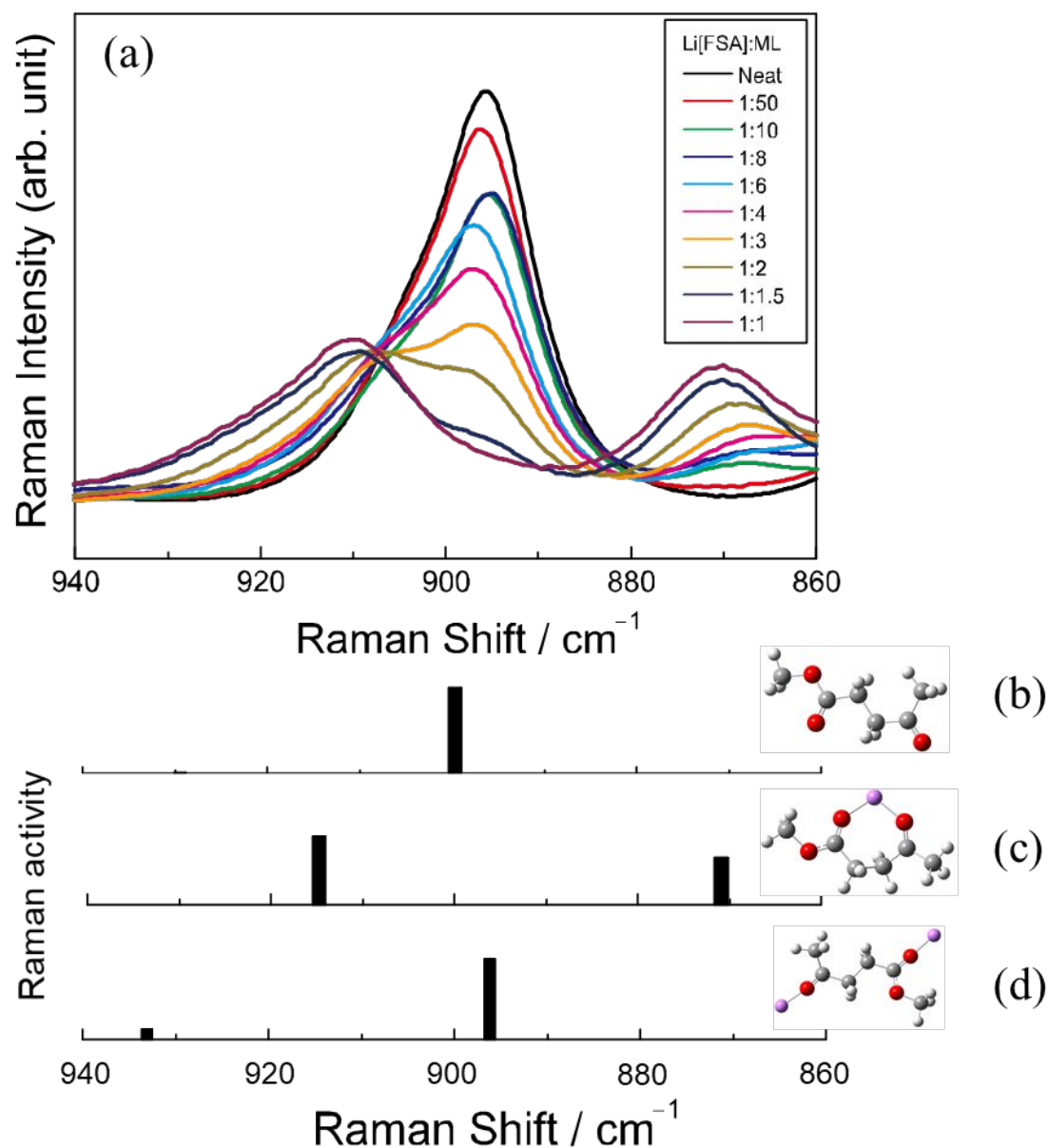


Figure 8. (a) Raman spectra of ML-based electrolytes at various Li[FSA]:ML ratios and calculated Raman bands of optimized structure for (b) neat ML, (c) bidentate Li⁺-ML (1:1), and (d) bridging Li⁺-ML (2:1), in the range of 860-940 cm^{-1} corresponding to the mixed modes of C-C stretching, CH₃ rocking and C-O stretching vibrations of ML.

Correlation between ion transport and coordination structure

Given the ionic diffusion behavior and Li ion coordination structure mentioned in the above sections, there seems to be a clear correlation between them. In MP- and MA-based concentrated electrolytes, for which Li⁺ showed the highest D values among the diffusive components, the presence of solvent-shared, extended chain-like structures, where solvent molecules coordinate to two different Li ions,

was strongly suggested by the single crystal structure of the model systems and the related Raman studies. FSA anions also participated in forming AGG or multi-ionic clusters with Li ions. These experimental findings are very similar to those for SL-based concentrated electrolytes: the fastest Li ion diffusion and the coexistence of SL-bridged chain-like structure and the anion-based AGG structure with Li ions.¹⁹ It is likely that, in AGG structures, Li ions and counter anions are transported both via an ion exchange mechanism as well as via a simple physical diffusion mechanism. In addition to these processes, Li ion transport can be further enhanced by a Li ion exchange mechanism through solvent-shared, extended chain-like structures, and that can be the cause of the most pronounced diffusion for Li ions relative to the solvent and anions in these concentrated electrolytes.

In ML-based concentrated electrolytes, the anion-based AGGs were found to be similar to the other keto ester-based concentrated electrolytes. However, the occurrence of the solvent bridged structure was less-pronounced because the bidentate ML apparently accounts for a large proportion of Li ion coordination. In this case, FSA anion was the fastest diffusive component. These behaviors are notably similar to those for the previously studied G3- and G4-based concentrated electrolyte of Li[FSA] with [glyme]/[Li] ratio lower than 1. For example, D_{FSA} was 5.6 times higher than D_{Li} at $[\text{G4}]/[\text{Li}] = 0.5$, and all the G4 molecules formed crown-ether like $[\text{Li}(\text{G4})]^+$ (1:1) complex cations, but no G4-based extended structure was found. The excess Li ions in G3- and G4-based concentrated electrolytes formed similar AGG structures with FSA anions.²⁸ In these systems, the multi-dentate solvents coordinating to one Li ion may terminate the ionic chain-like structures based on either ML or FSA with Li ions, leading to less-pronounced solvent bridged structures. Although Li ions and anions can be equally transported through the ion exchange mechanism in AGG structures, an additional Li ion

exchange mechanism is unlikely due to lack of the solvent-shared, extended structures. Rather, Li ions are more prone to diffusing via a vehicle-type mechanism in the form of complex cations with multi-dentate solvents. Since PFG-NMR detects the averaged diffusion coefficient, the vehicle-type diffusion of larger Li complex ions contributes to the decrease in D_{Li} , and thereby D_{FSA} was shown to be higher than D_{Li} in ML- and glyme-based concentrated electrolytes.

Conclusion

To clarify the key factors behind the Li ion hopping or exchange mechanism in liquid electrolytes, the correlation between ionic diffusion behavior and Li ion coordination was studied in keto ester-based concentrated electrolytes. Diffusivity measurements by PFG-NMR indicated that Li ions are the fastest among the components in MP- and MA-based concentrated electrolytes whereas FSA anions are the fastest in the corresponding ML-based solutions. These results are indicative of the contribution of a Li ion hopping/exchange mechanism to the ion transport in the keto ester-based concentrated electrolytes. Studies on the single crystal structure and Raman spectra of the related Li-solvent complexes suggested that a solvent-bridged, chain-like Li ion coordination and AGG of Li ions and FSA anions coexist in MP- and MA-based electrolytes, whereas the solvent-bridged structure is less-pronounced and AGG is present as a predominant ionic network in ML-based electrolytes. Which ionic species are faster was suggested to be determined by the presence or absence of the solvent-bridged, chain-like Li ion coordination. The Li ion hopping/exchange dominated transport can be attributed to liquid electrolytes with both the solvent-bridged, chain-like Li ion coordination and AGG or ionic clusters although these considerations need to be verified by further MD simulations in the

future. The extent to which the observed Li ion hopping diffusion in the bulk electrolytes affect the actual Li ion flux in the presence of an electric field and concentration gradient in an electrochemical device is not yet understood in detail. However, the significance of the labile Li ion coordination network with the solvent bridging and its correlation with Li ion hopping diffusion found in this work provides an insight into the design of superionic liquid electrolytes in which Li ion transport can be decoupled from viscosity-dominated diffusion processes.

Conflicts of interest

There are no conflicts to declare.

Acknowledgements

This study was supported in part by the JSPS KAKENHI (Grant Nos. 16H06053 to K.U., 18K14310 to T.M., 18H03926 to K.D. and 15H05758 to M.W.) from the Japan Society for the Promotion of Science (JSPS), and the Advanced Low Carbon Technology Research and Development Program (ALCA) of the Japan Science and Technology Agency (JST). The authors wish to acknowledge Prof. Yoshitaka Yamaguchi, and Dr. Yutaro Kamei for their helpful comments on X-ray crystallography.

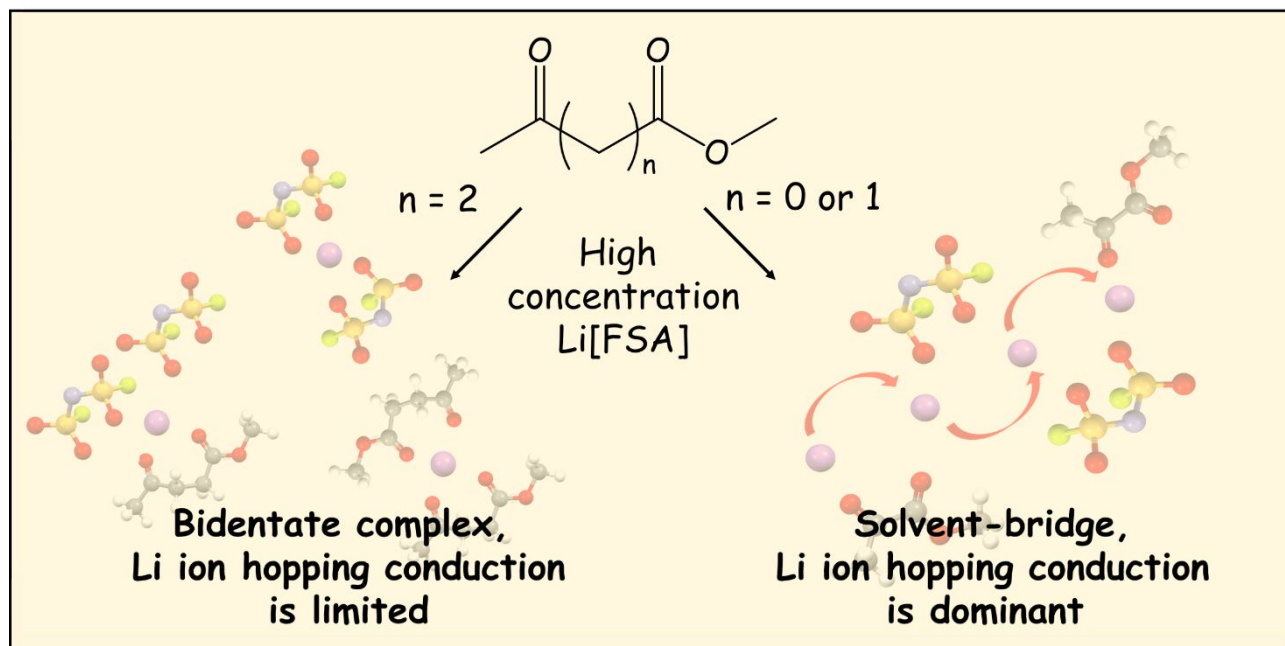
Supplementary Information: Li^+ transference number. Details of single crystals at $\text{Li}[\text{FSA}]:\text{MP}=1:0.5$, $\text{Li}[\text{FSA}]:\text{MP} = 1:2$, and $\text{Li}[\text{TFSA}]:\text{MA}=1:0.5$. Raman spectra for MP- and MA-based electrolytes ($1600\text{-}1800\text{ cm}^{-1}$), for solid $\text{Li}[\text{FSA}]$ and MP-based electrolytes at $[\text{MP}]/[\text{Li}] = 0.5$ ($780\text{-}900\text{ cm}^{-1}$), for FSA anions ($720\text{-}760\text{ cm}^{-1}$), and for ML-based electrolytes ($700\text{-}850\text{ cm}^{-1}$).

References

1. N. Kamaya, K. Homma, Y. Yamakawa, M. Hirayama, R. Kanno, M. Yonemura, T. Kamiyama, Y. Kato, S. Hama, K. Kawamoto and A. Mitsui, *Nat. Mater.*, 2011, **10**, 682-686.
2. Y. Seino, T. Ota, K. Takada, A. Hayashi and M. Tatsumisago, *Energy Environ. Sci.*, 2014, **7**, 627-631.
3. Y. Kato, S. Hori, T. Saito, K. Suzuki, M. Hirayama, A. Mitsui, M. Yonemura, H. Iba and R. Kanno, *Nat. Energy*, 2016, **1**, 7.
4. Y. Yamada and A. Yamada, *J. Electrochem. Soc.*, 2015, **162**, A2406-A2423.
5. D. W. McOwen, D. M. Seo, O. Borodin, J. Vatamanu, P. D. Boyle and W. A. Henderson, *Energy Environ. Sci.*, 2014, **7**, 416-426.
6. K. Yoshida, M. Nakamura, Y. Kazue, N. Tachikawa, S. Tsuzuki, S. Seki, K. Dokko and M. Watanabe, *J. Am. Chem. Soc.*, 2011, **133**, 13121-13129.
7. Y. Yamada, K. Furukawa, K. Sodeyama, K. Kikuchi, M. Yaegashi, Y. Tateyama and A. Yamada, *J. Am. Chem. Soc.*, 2014, **136**, 5039-5046.
8. Y. Yamada, M. Yaegashi, T. Abe and A. Yamada, *Chem. Commun.*, 2013, **49**, 11194-11196.
9. J. Wang, Y. Yamada, K. Sodeyama, C. H. Chiang, Y. Tateyama and A. Yamada, *Nat. Commun.*, 2016, **7**, 12032.
10. J. Qian, W. A. Henderson, W. Xu, P. Bhattacharya, M. Engelhard, O. Borodin and J.-G. Zhang, *Nat. Commun.*, 2015, **6**, 6362.
11. R. Petibon, C. P. Aiken, L. Ma, D. Xiong and J. R. Dahn, *Electrochim. Acta*, 2015, **154**, 287-293.
12. L. Suo, W. Xue, M. Gobet, S. G. Greenbaum, C. Wang, Y. Chen, W. Yang, Y. Li and J. Li, *Proc. Natl. Acad. Sci. USA*, 2018, **115**, 1156-1161.
13. D. M. Seo, O. Borodin, D. Balogh, M. O'Connell, Q. Ly, S.-D. Han, S. Passerini and W. A. Henderson, *J. Electrochem. Soc.*, 2013, **160**, A1061-A1070.
14. O. Borodin, G. A. Giffin, A. Moretti, J. B. Haskins, J. W. Lawson, W. A. Henderson and S. Passerini, *J. Phys. Chem. C*, 2018, **122**, 20108-20121.
15. M. Callsen, K. Sodeyama, Z. Futera, Y. Tateyama and I. Hamada, *J. Phys. Chem. B*, 2017, **121**, 180-188.
16. M. Forsyth, H. Yoon, F. Chen, H. Zhu, D. R. MacFarlane, M. Armand and P. C. Howlett, *J. Phys. Chem. C*, 2016, **120**, 4276-4286.
17. M. Brinkkotter, G. A. Giffin, A. Moretti, S. Jeong, S. Passerini and M. Schonhoff, *Chem. Commun.*, 2018, **54**, 4278-4281.
18. H. Yoon, P. C. Howlett, A. S. Best, M. Forsyth and D. R. MacFarlane, *J. Electrochem. Soc.*, 2013, **160**, A1629-A1637.
19. K. Dokko, D. Watanabe, Y. Ugata, M. L. Thomas, S. Tsuzuki, W. Shinoda, K. Hashimoto, K. Ueno, Y. Umabayashi and M. Watanabe, *J. Phys. Chem. B*, 2018, **122**, 10736-10745.

20. J. Alvarado, M. A. Schroeder, M. Zhang, O. Borodin, E. Gobrogge, M. Olguin, M. S. Ding, M. Gobet, S. Greenbaum, Y. S. Meng and K. Xu, *Mater. Today*, 2018, **21**, 341-353.
21. C. S. Johnson, *Prog. Nucl. Magn. Reson. Spectrosc.*, 1999, **34**, 203-256.
22. D. Sinnaeve, *Concept Magn. Reson. A*, 2012, **40A**, 39-65.
23. M. J. Frisch, G. W. Trucks, H. B. Schlegel, G. E. Scuseria, M. A. Robb, J. R. Cheeseman, G. Scalmani, V. Barone, B. Mennucci, G. A. Petersson, H. Nakatsuji, M. Caricato, X. Li, H. P. Hratchian, A. F. Izmaylov, J. Bloino, G. Zheng, J. L. Sonnenberg, M. Hada, M. Ehara, K. Toyota, R. Fukuda, J. Hasegawa, M. Ishida, T. Nakajima, Y. Honda, O. Kitao, H. Nakai, T. Vreven, J. A. Montgomery, J. E. Peralta, F. Ogliaro, M. Bearpark, J. J. Heyd, E. Brothers, K. N. Kudin, V. N. Staroverov, R. Kobayashi, J. Normand, K. Raghavachari, A. Rendell, J. C. Burant, S. S. Iyengar, J. Tomasi, M. Cossi, N. Rega, J. M. Millam, M. Klene, J. E. Knox, J. B. Cross, V. Bakken, C. Adamo, J. Jaramillo, R. Gomperts, R. E. Stratmann, O. Yazyev, A. J. Austin, R. Cammi, C. Pomelli, J. W. Ochterski, R. L. Martin, K. Morokuma, V. G. Zakrzewski, G. A. Voth, P. Salvador, J. J. Dannenberg, S. Dapprich, A. D. Daniels, Farkas, J. B. Foresman, J. V. Ortiz, J. Cioslowski and D. J. Fox, *Journal*, 2009, DOI: citeulike-article-id:9096580.
24. O. V. Dolomanov, L. J. Bourhis, R. J. Gildea, J. A. K. Howard and H. Puschmann, *J. Appl. Crystallogr.*, 2009, **42**, 339-341.
25. J. Lee, Y. Lee, J. Lee, S.-M. Lee, J.-H. Choi, H. Kim, M.-S. Kwon, K. Kang, K. T. Lee and N.-S. Choi, *ACS Appl. Mater. Interface*, 2017, **9**, 3723-3732.
26. S.-D. Han, O. Borodin, D. M. Seo, Z.-B. Zhou and W. A. Henderson, *J. Electrochem. Soc.*, 2014, **161**, A2042-A2053.
27. S. Terada, H. Susa, S. Tsuzuki, T. Mandai, K. Ueno, K. Dokko and M. Watanabe, *J. Phys. Chem. C*, 2018, **122**, 16589-16599.
28. S. Terada, K. Ikeda, K. Ueno, K. Dokko and M. Watanabe, *Aust. J. Chem.*, 2018, DOI: <https://doi.org/10.1071/CH18270>, -.
29. K. Hayamizu, Y. Aihara, S. Arai and C. G. Martinez, *J. Phys. Chem. B*, 1999, **103**, 519-524.
30. C. Capiglia, Y. Saito, H. Kageyama, P. Mustarelli, T. Iwamoto, T. Tabuchi and H. Tukamoto, *J. Power Sources*, 1999, **81**, 859-862.
31. R. Tataru, D. G. Kwabi, T. P. Batcho, M. Tulodziecki, K. Watanabe, H.-M. Kwon, M. L. Thomas, K. Ueno, C. V. Thompson, K. Dokko, Y. Shao-Horn and M. Watanabe, *J. Phys. Chem. C*, 2017, **121**, 9162-9172.
32. C. Zhang, K. Ueno, A. Yamazaki, K. Yoshida, H. Moon, T. Mandai, Y. Umebayashi, K. Dokko and M. Watanabe, *J. Phys. Chem. B*, 2014, **118**, 5144-5153.
33. O. Borodin, L. Suo, M. Gobet, X. Ren, F. Wang, A. Faraone, J. Peng, M. Olguin, M. Schroeder, M. S. Ding, E. Gobrogge, A. von Wald Cresce, S. Munoz, J. A. Dura, S. Greenbaum, C. Wang and K. Xu, *ACS Nano*, 2017, **11**, 10462-10471.
34. C. J. Jafta, C. Bridges, L. Haupt, C. Do, P. Sippel, M. J. Cochran, S. Krohns, M. Ohl, A. Loidl, E. Mamontov, P. Lunkenheimer, S. Dai and X. G. Sun, *ChemSusChem*, 2018, **11**, 3512-3523.
35. K.-D. Kreuer, *Chem. Mater.*, 1996, **8**, 610-641.
36. K. Fujii, H. Hamano, H. Doi, X. Song, S. Tsuzuki, K. Hayamizu, S. Seki, Y. Kameda, K. Dokko, M. Watanabe and Y. Umebayashi, *J. Phys. Chem. C*, 2013, **117**, 19314-19324.
37. J. Wilmshurst and J. Horwood, *Aust. J. Chem.*, 1971, **24**, 1183-1191.
38. H. Yoon, A. S. Best, M. Forsyth, D. R. MacFarlane and P. C. Howlett, *Phys Chem Chem Phys*, 2015, **17**, 4656-4663.

39. M. M. Schiavoni, H. E. Di Loreto, A. Hermann, H.-G. Mack, S. E. Ulic and C. O. Della Védova, *J. Raman Spectrosc.*, 2001, **32**, 319-329.
40. Y. Pocker and G. T. Spyridis, *J. Am. Chem. Soc.*, 2002, **124**, 10373-10380.

Table of contents entry:

The hopping/exchange-dominated Li ion transport is attributed to liquid electrolytes with solvent-bridged, chain-like Li ion coordination and aggregated ion pairs.